JOURNAL OF MATERIALS SCIENCE **36** (2001) 643–651

The effect of Nb addition on microstructure and mechanical properties of $Ni_3(Si,Ti)$ alloy

T. TAKASUGI
Department of Metallurgy and Materials Science, College of Engineering, Osaka Prefecture University, Gakuen-cho, 1-1, Sakai, Osaka, 599-8531, Japan
E-mail: takasugi@mtl.osakafu-u.ac.jp

M. YOSHIDA
Miyagi National College of Technology, Natori, Miyagi Prefecture, 981-1239, Japan

The alloying behavior, the microstructure and the high-temperature tensile properties of the Nb-added $Ni_3(Si,Ti)$ alloys were investigated. The solubility limit of Nb element in the $L1_2$ $Ni_3(Si,Ti)$ phase at 1273 K was shown to be approximately 2.7 at%, and thermodynamically discussed. The second-phases (dispersions) formed beyond the solubility limits were identified as $D0_a$-type Ni_3Nb and $Ni_{12}Si_4TiNb_2$ compounds, and contained some lattice defects with incoherency with the $L1_2$ $Ni_3(Si,Ti)$ matrix. The Nb-containing second-phase dispersions in the $L1_2$ $Ni_3(Si,Ti)$ phase matrix resulted in strengthening over a wide range of temperature, and also an improvement of the high-temperature tensile elongation. © *2001 Kluwer Academic Publishers*

1. Introduction

Ni_3Si has been considered to be a candidate as a high-temperature structural material and especially chemical parts because Ni_3Si displays an increasing strength with increasing temperature and also shows excellent oxidation and corrosion resistance over a wide range of temperature. Ti has a relatively large solubility limit ($\sim$11 at%) in the $L1_2$ Ni_3Si phase [1]. Ti additions to the Ni_3Si resulted in a number of useful mechanical properties: an increased strength as a result of its solid solution hardening, and also a high tensile ductility over a wide range of temperatures by reducing the propensity to intergranular fracture [2]. Also, Ti addition enhanced the peak temperature in the strength vs. temperature curve through modifying the specific dislocation structure [3, 4].

To improve further the mechanical and related properties of the $Ni_3(Si,Ti)$ alloy, alloying methods have been carried out. For examples, doping with interstitials such as boron, carbon and beryllium has been shown to improve the ambient tensile ductility via reducing the propensity to the intergranular fracture [5–7]. Also, it has been reported that addition of some substitutional (transition) metals to the $Ni_3(Si,Ti)$ alloy improved the mechanical properties (e.g. increased strength over a wide range of temperature) mostly within their maximum solubility limits [8]. Among the transition metals, Nb has been reported to have a secondly largest solubility limit in the $L1_2$ Ni_3Si phase [9]. In the present study, the alloying behavior, the microstructure and the high-temperature tensile properties of the Nb-added $Ni_3(Si,Ti)$ alloys were investigated by optical microscopy, x-ray diffraction, scanning microscopy attached with electron probe analysis, transmission electron microscopy and tensile testing. Nb was added to the $Ni_3(Si,Ti)$ alloy up to concentrations exceeding the solubility limit in the $L1_2$ $Ni_3(Si,Ti)$ phase. It is shown that the $Ni_3(Si,Ti)$ alloy, with a duplex microstructure consisting of the $L1_2$ phase and Nb-containing second-phase dispersions, has excellent mechanical properties over a wide range of temperature.

2. Experimental procedure

Quaternary element Nb was added to $Ni_{79.5}Si_{11}Ti_{9.5}$ (denoted by at%) alloy composition such that the Nb element substitutes for Ti sites, keeping the concentration of the other constituents Ni and Si constant. Therefore, quaternary alloys with a nominal composition of $Ni_{79.5}Si_{11}Ti_{9.5-x}Nb_x$ were prepared in this study, starting from raw materials of 99.9 wt%Ni, 99.999 wt%Si, 99.9 wt%Ti and 99.5 wt%Nb. Alloy ingots with dimensions $50 \times 30 \times 15$ mm^3 were prepared by non-consumable arc melting in argon gas on copper hearth. The alloy ingots were homogenized at 1323 K for 1 day in vacuum, and then cut into several plates. These plates were repeatedly rolled at 573 K in air and annealed in vacuum at 1273 K. Final thickness of the rolled plates was approximately 1 mm.

Metallographic, chemical and structural observations of the Nb-added $Ni_3(Si,Ti)$ alloys were carried out to study the recrystallized microstructures by optical microscopy (OM), x-ray diffraction (XRD), scanning electron microscopy (SEM) attached with wave-length dispersive spectroscopy (WDS) and transmission electron microscopy (TEM). X-ray diffraction profiles were obtained using Cu K_α radiation. The WDS data for alloy compositions of the $L1_2$ matrix and the second-phases

(dispersions) were collected from more than five areas and then averaged. Crystal structures of the second-phase dispersions were determined on the basis of the x-ray diffraction and the WDS analysis in SEM observation. Thin foil specimens for TEM observation were prepared by electropolising in a solution of 10% H_2SO_4 and 90% CH_3OH at 273 K. TEM observation was made using a JEOL electron microscope operating at 200 kV.

Tensile specimens with a gauge dimension of $14 \times 2 \times 1$ mm^3 were prepared by electrodischarge machining (EDM) from the rolled plates, and subsequently annealed for 5 h at 1273 K in vacuum to obtain recrystallized microstructures. The tensile tests were conducted in vacuum in the temperature range between room temperature and 1073 K, using an Instron-type testing machine at a nominal strain rate of 1.2×10^{-3} s^{-1}. The faces of the tensile specimens were abraded with a sufficiently fine SiC paper before the tensile test. Fracture surfaces of the deformed specimens were examined by scanning electron microscopy (SEM).

3. Results

3.1. Alloying behavior and microstructure

SEM microstructure of the Nb-added $Ni_3(Si,Ti)$ alloys with concentrations less than 2 at%Nb showed an $L1_2$ single phase, while those with concentrations more than 3 at%Nb showed duplex microstructures consisting of $L1_2$ phase and second-phase dispersions, as shown in Fig. 1. Consequently, the solubility limit of the Nb element in the $L1_2$ $Ni_3(Si,Ti)$ matrix at 1273 K was postulated to lie between 2 at% and 3 at% Nb. The 2 at%Nb-added $Ni_3(Si,Ti)$ alloy exhibits equiaxed grains with a grain size of about 25 μm, accompanied with a number of annealing twins. This microstructure is very similar to that of the unalloyed (i.e. ternary) $Ni_3(Si,Ti)$, that has repeatedly been reported in previous studies [1, 2, 5–7]. On the other hand, the 4 at% Nb-added $Ni_3(Si,Ti)$ alloy exhibits two types of second-phase dispersions within the $L1_2$ $Ni_3(Si,Ti)$ matrix; one is relatively large rounded second-phase dispersions with a volume fraction of about 23%, while another is irregularly shaped second-phase dispersions with a volume fraction of less than 5%. Their sizes were widely distributed. However, it was found that the second-phase dispersions primarily did not affect grain morphology but slightly reduced the grain size of the $L1_2$ phase matrix.

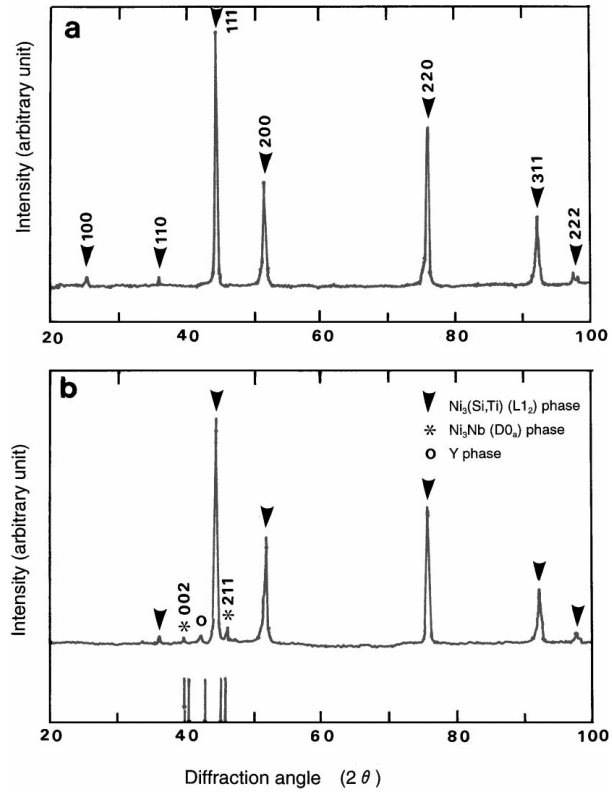

Figure 2 X-ray diffraction profiles of (a) the 2 at% Nb and (b) the 4 at% Nb-added $Ni_3(Si,Ti)$ alloys. Note that theoretical diffraction peaks from the $D0_a$–type Ni_3Nb structure are included into the x-ray profile of the 4 at% Nb-added $Ni_3(Si,Ti)$ alloy.

Fig. 2 shows x-ray diffraction profiles of the 2 at% Nb and 4 at% Nb-added $Ni_3(Si,Ti)$ alloys. Corresponding to the SEM microstructures, all the diffraction peaks were determined as the $L1_2$ structure for the 2 at%Nb-added $Ni_3(Si,Ti)$ alloy. On the other hand, additional diffraction peaks from the second-phase dispersions were observed for the 4 at%Nb-added $Ni_3(Si,Ti)$ alloy. Some of those diffraction peaks were identified as $D0_a$–type Ni_3Nb structure, conference with the WDS analysis. Here, the experimental diffraction angles from the $D0_a$–type Ni_3Nb structure were slightly deviated from their theoretical diffraction angles. This difference may be due to the presence of the other constituents Si and Ti that are moderately soluble in the Ni_3Nb phase and consequently changed the lattice parameter, as will

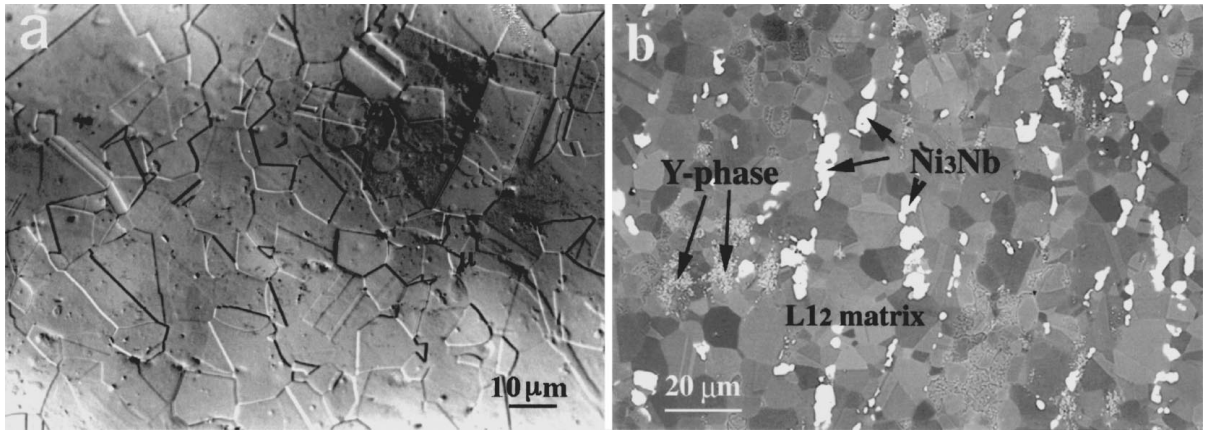

Figure 1 SEM microstructures of (a) the 2 at% Nb and (b) the 4 at% Nb-added $Ni_3(Si,Ti)$ alloys.

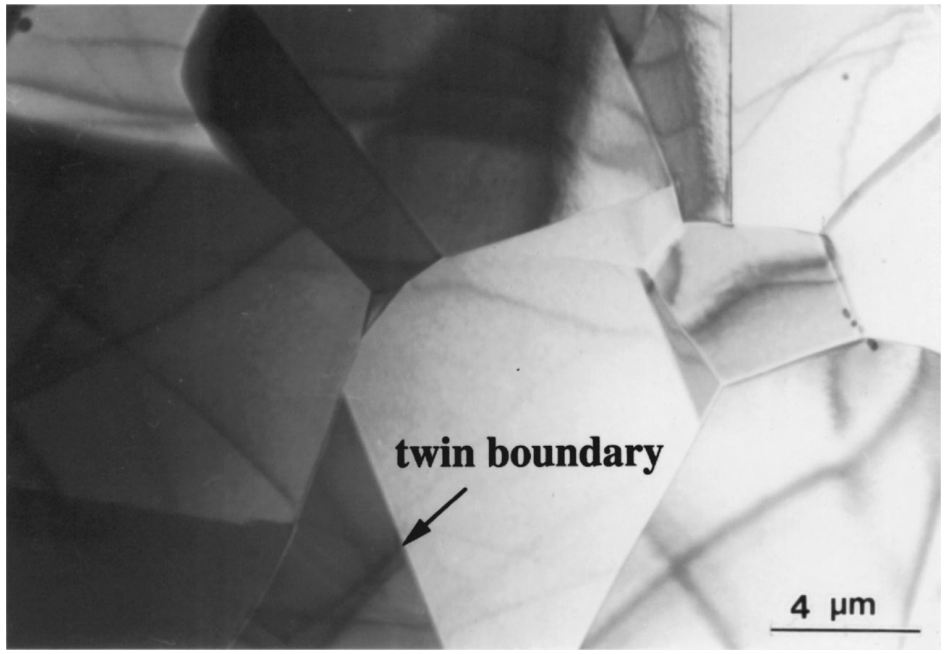

Figure 3 TEM microstructure of the 2 at% Nb-added $Ni_3(Si,Ti)$ alloy.

be mentioned later. Remaining diffraction peaks were identified as neither $L1_2$ structure nor $D0_a$–type Ni_3Nb structure, and therefore defined as Y-phase. However, the crystal structure of the Y-phase was not determined because of an insufficient number of the diffraction peaks. A separated study is undertaken to determine the crystal structure of the Y-phase.

Figs 3 and 4 show the TEM (or SEM) microstructures of the 2 at% Nb and the 4 at% Nb-added $Ni_3(Si,Ti)$ alloys observed at high magnification, respectively. The 2 at%Nb-added $Ni_3(Si,Ti)$ alloy showed equiaxed grains composed of large-angle boundaries and twin boundaries. Also, extra spots in SADP showed an indication of the ordered structure. On other hand, the 4 at%Nb-added $Ni_3(Si,Ti)$ alloy showed rounded second-phase dispersions (Fig. 4a) and irregularly shaped second-phase dispersions (Fig. 4b) within the $L1_2$ grains. Characteristic images were observed within the $D0_a$–type Ni_3Nb second-phase dispersions. Planar defect-like images (Fig. 5a) and dislocation-like images (Fig. 5b) were occasionally observed within the second-phase dispersions. At the moment, whether such lattice defects were introduced during solidification or during solid-state processing (i.e. rolling and subsequent annealing) is not evident. Detailed TEM observation is undertaken into an extending study and will be published in a separate literature. Interface structure between the $L1_2$ $Ni_3(Si,Ti)$ matrix and the $D0_a$-type Ni_3Nb second-phase dispersion was also observed by TEM as shown in Fig. 5b. There were not any specific orientation relationships and interface structures between the two structures. Thus, interface was primarily incoherent and did not show any habit planes.

Alloy compositions of the constituent phases for the 4 at%Nb-added $Ni_3(Si,Ti)$ alloy was determined by SEM-WDS. The $L1_2$ $Ni_3(Si,Ti)$ phase matrix consisted of an alloy with a composition of 79.1 at% Ni, 12.3 at% Si, 5.9 at% Ti and 2.7 at% Nb. The solubility limit of the Nb in the $Ni_3(Si,Ti)$ at 1273 K is determined to be ~2.7 at%. On the other hand, the $D0_a$–type Ni_3Nb second-phase dispersion consisted of an alloy with a composition of 69.3 at% Ni, 7.7 at% Si, 2.8 at% Ti and 20.1 at% Nb while the Y-phase dispersion consisted of an alloy with a composition of 58.8 at% Ni, 22.0 at% Si, 7.0 at% Ti and 12.2 at% Nb. Therefore, the Y-phase can be described as $Ni_{12}Si_4TiNb_2$. The both types of dispersed second-phases contain Ni and Nb as the major constituents.

3.2. High-temperature tensile properties

Fig. 6 plots the yield stress (defined at 0.2% offset strain) of the Nb-added $Ni_3(Si,Ti)$ alloys as a function of test temperature. Here, the data for the unalloyed $Ni_3(Si,Ti)$ (which was fabricated in a similar way to the present alloys and tested under similar experimental conditions) are from previous work [5]. The yield stress increased from room temperature with increasing temperature, reached a maximum and then decreased rapidly with further increase in temperature. The peak temperatures of the yield stress occurred at 873 K and 673 K for the 2 at%Nb and the 4 at%Nb-added $Ni_3(Si,Ti)$ alloys, respectively.

The yield stress was enhanced by the Nb addition particularly at low temperatures. The yield stress increases in the 2 at%Nb-added $Ni_3(Si,Ti)$ alloy can be attributed to the solid solution strengthening in the $L1_2$ $Ni_3(Si,Ti)$ matrix. On the other hand, that in the 4 at%Nb-added $Ni_3(Si,Ti)$ alloy can be attributed to the second-phase dispersion strengthening (plus the solid solution strengthening in the $L1_2$ $Ni_3(Si,Ti)$ matrix). The positive temperature dependence of the yield stress appears to decrease in the two Nb-added $Ni_3(Si,Ti)$ alloys.

Fig. 7 plots the tensile elongation of the Nb-added $Ni_3(Si,Ti)$ alloys as a function of test temperature. It has been reported in the previous work that the tensile elongation of the unalloyed $Ni_3(Si,Ti)$ rapidly decreased from room temperature and becomes zero at

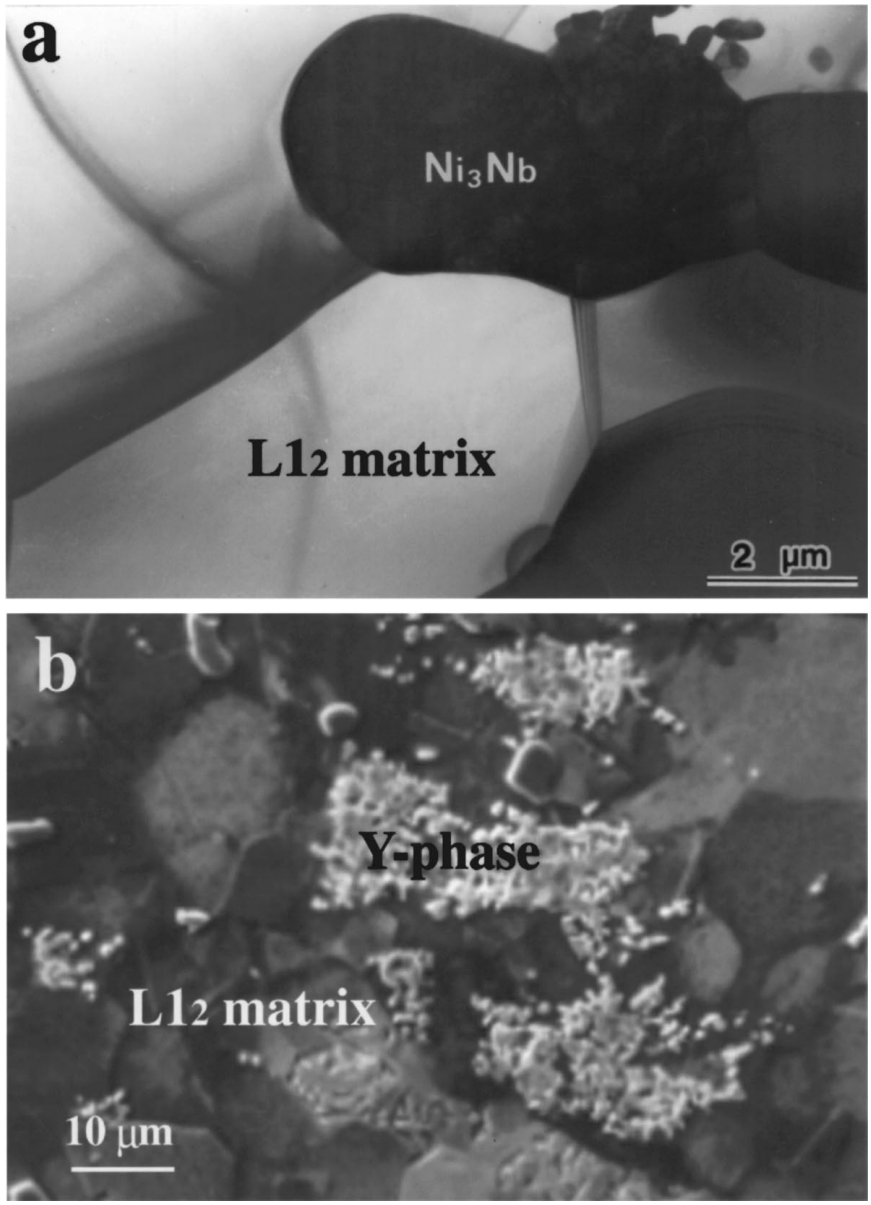

Figure 4 (a) TEM and (b) SEM microstructures of the 4 at% Nb-added $Ni_3(Si,Ti)$ alloy. The $D0_a$–type Ni_3Nb dispersion and the Y-phase dispersion defined as $Ni_{12}Si_4TiNb_2$ are shown in (a) and (b), respectively.

temperatures above 673 K [5]. By the 2 at%Nb addition, the tensile elongation of the $Ni_3(Si,Ti)$ alloy was significantly improved over a wide range of temperature although the room temperature tensile elongation was slightly reduced. The tensile elongation of the 2 at%Nb-added $Ni_3(Si,Ti)$ alloy showed the values beyond 20% up to 673 K, began to decrease above 673 K and eventually was zero at temperatures above 973 K. Striking result was observed for the 4 at%Nb-added $Ni_3(Si,Ti)$ alloy with second-phase (i.e. hard) dispersions. The tensile elongation of the 4 at%Nb-added $Ni_3(Si,Ti)$ alloy showed lower values at low temperatures (i.e. room temperature and 473 K) than that of the unalloyed $Ni_3(Si,Ti)$. However, the tensile elongation at high temperatures (i.e. $>$473 K) was significantly improved. In addition, the tensile elongation at the highest temperature ($\sim$1073 K) tended to increase from the elongation minimum appearing at an intermediate temperature.

Fig. 8 plots the ultimate tensile stress (UTS) of the Nb-added $Ni_3(Si,Ti)$ alloys as a function of test temperature. It has been reported in the previous work that the UTS of the unalloyed $Ni_3(Si,Ti)$ decreased rapidly above room temperature and became zero at temperatures above 673 K [5]. These UTS results appear to be correlated well with the tensile elongation results. The two Nb-added $Ni_3(Si,Ti)$ alloy displayed consistently higher UTS values than the unalloyed $Ni_3(Si,Ti)$ over a wide range of temperature. In the high temperature region ($>$673 K), the 4 at%Nb-added $Ni_3(Si,Ti)$ alloy displayed higher UTS than the 2 at%Nb-added $Ni_3(Si,Ti)$.

3.3. Fractography

Figs 9 and 10 show the effect of test temperature on fracture surface for the 2 at%Nb and the 4 at%Nb-added $Ni_3(Si,Ti)$ alloys, respectively. For the 2 at%Nb-added $Ni_3(Si,Ti)$ alloy, transgranular fracture with dimple patterns dominated at room temperature, with a small portion of intergranular fracture (Fig. 9a). At 673 K, transgranular fracture pattern dominated in almost all areas

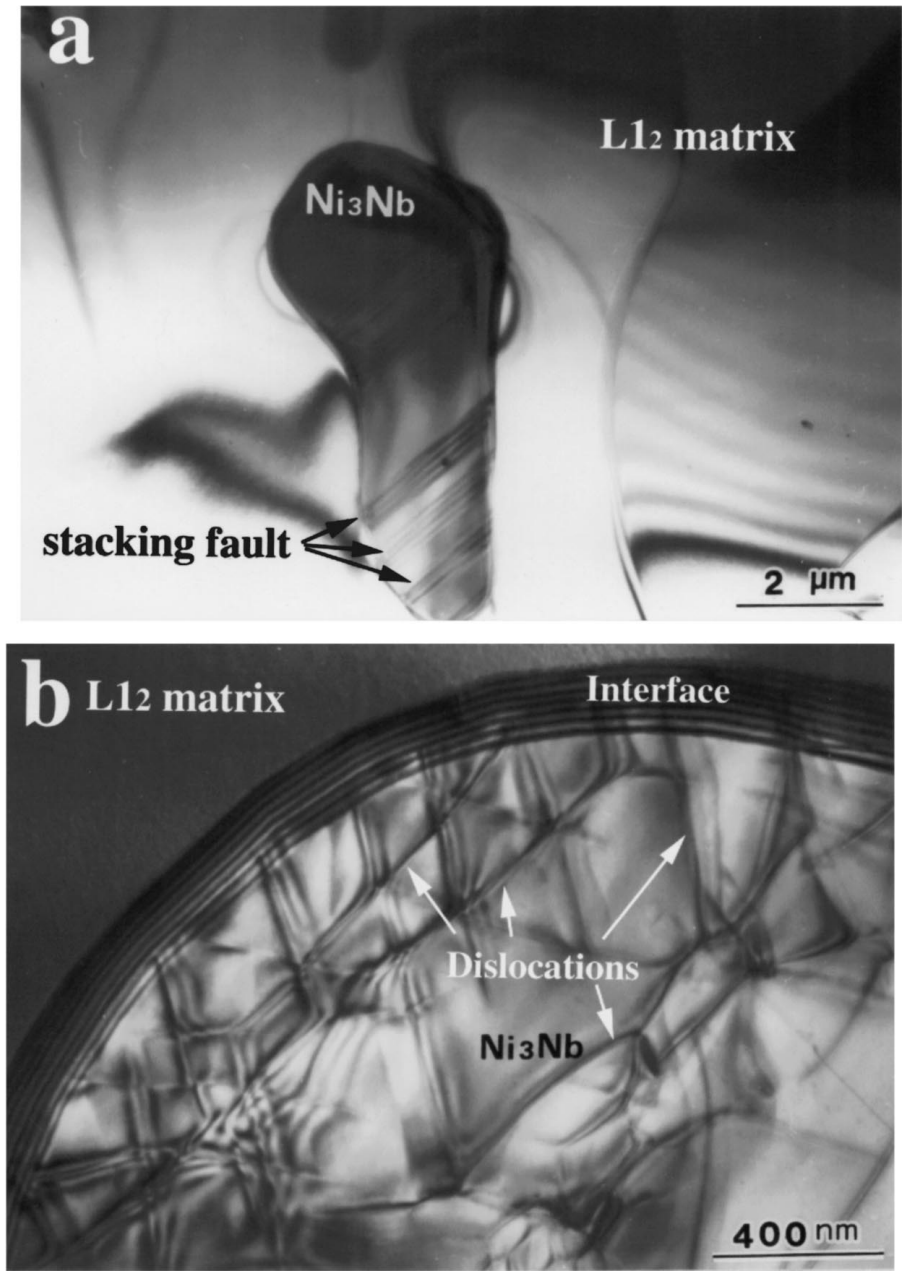

Figure 5 (a) and (b): TEM images of the $D0_a$–type Ni_3Nb second-phase dispersions in the 4 at% Nb-added $Ni_3(Si,Ti)$ alloy.

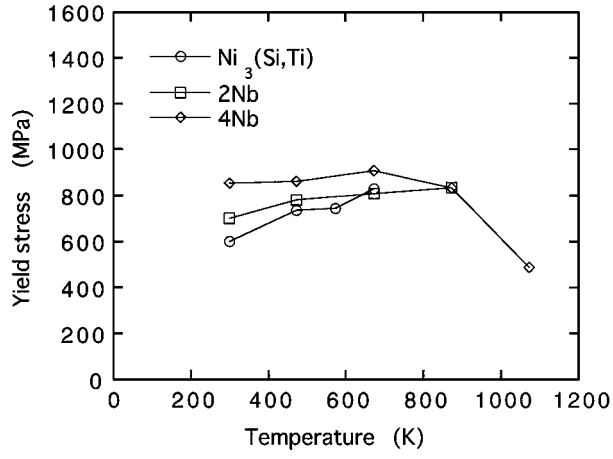

Figure 6 Yield stress of the Nb-added $Ni_3(Si,Ti)$ alloys as a function of test temperature. Testing was carried out in vacuum at a strain rate of 1.2×10^{-3} s^{-1}. Note that the data of the unalloyed $Ni_3(Si,Ti)$ at high temperatures are not obtained because the fracture occurred at stress levels below their macroscopic yielding.

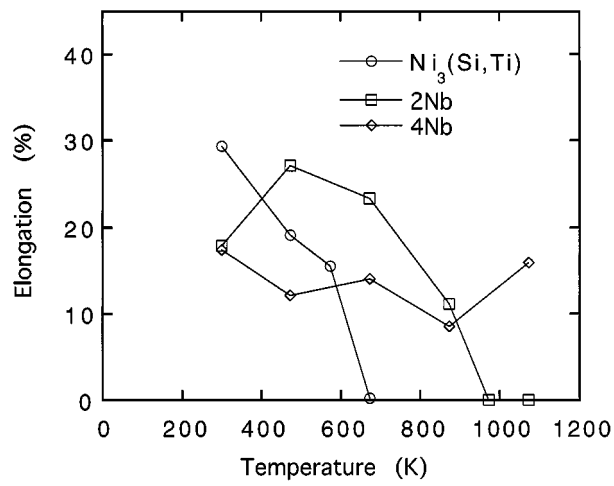

Figure 7 Tensile elongation of the Nb-added $Ni_3(Si,Ti)$ alloys as a function of test temperature. Testing was carried out in vacuum at a strain rate of 1.2×10^{-3} s^{-1}.

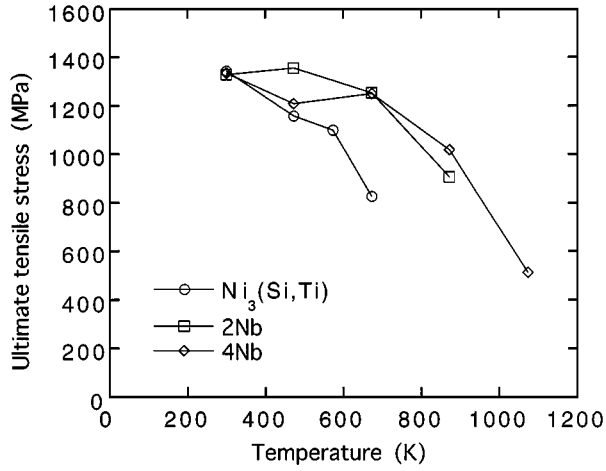

Figure 8 Ultimate tensile stress of the Nb-added $Ni_3(Si,Ti)$ alloys as a function of test temperature. Testing was carried out in vacuum at a strain rate of 1.2×10^{-3} s^{-1}.

(Fig. 9b). Corresponding to this result, largest tensile elongation and UTS values were observed. At temperatures above 673 K, intergranular fracture patterns became more dominant with increasing temperature, as shown in Fig. 9c. This variation of fracture mode with test temperature correlates well with the variations of the tensile elongation and UTS with temperature (Figs 7 and 8), that is, the more transgranular fracture mode the higher was the tensile elongation and UTS. For the 4 at%Nb-added $Ni_3(Si,Ti)$ alloy, the fracture patterns appear to be more temperature independent (Fig. 10). For all temperatures, transgranular fracture patterns with second-phase dispersions were observed in a mixture with a small portion of intergranular fracture patterns.

The increase in the tensile elongation of the 4 at%Nb-added $Ni_3(Si,Ti)$ alloy observed at the highest temperature (i.e. 1073 K) may be attributed to dynamic recrystallization taking place preferentially around the second-phase dispersions or prior grain boundaries. Fig. 11 shows fracture pattern taken at a high magnification in the 4 at%Nb-added $Ni_3(Si,Ti)$ alloy deformed at 1073 K. It is apparent that a number of small recrystallized new grains are observed on fracture pattern. Also, a cross-sectional view in a region close to the fracture surface indicates that a number of new grains were recrystallized at the second-phase dispersions or the prior grain boundaries.

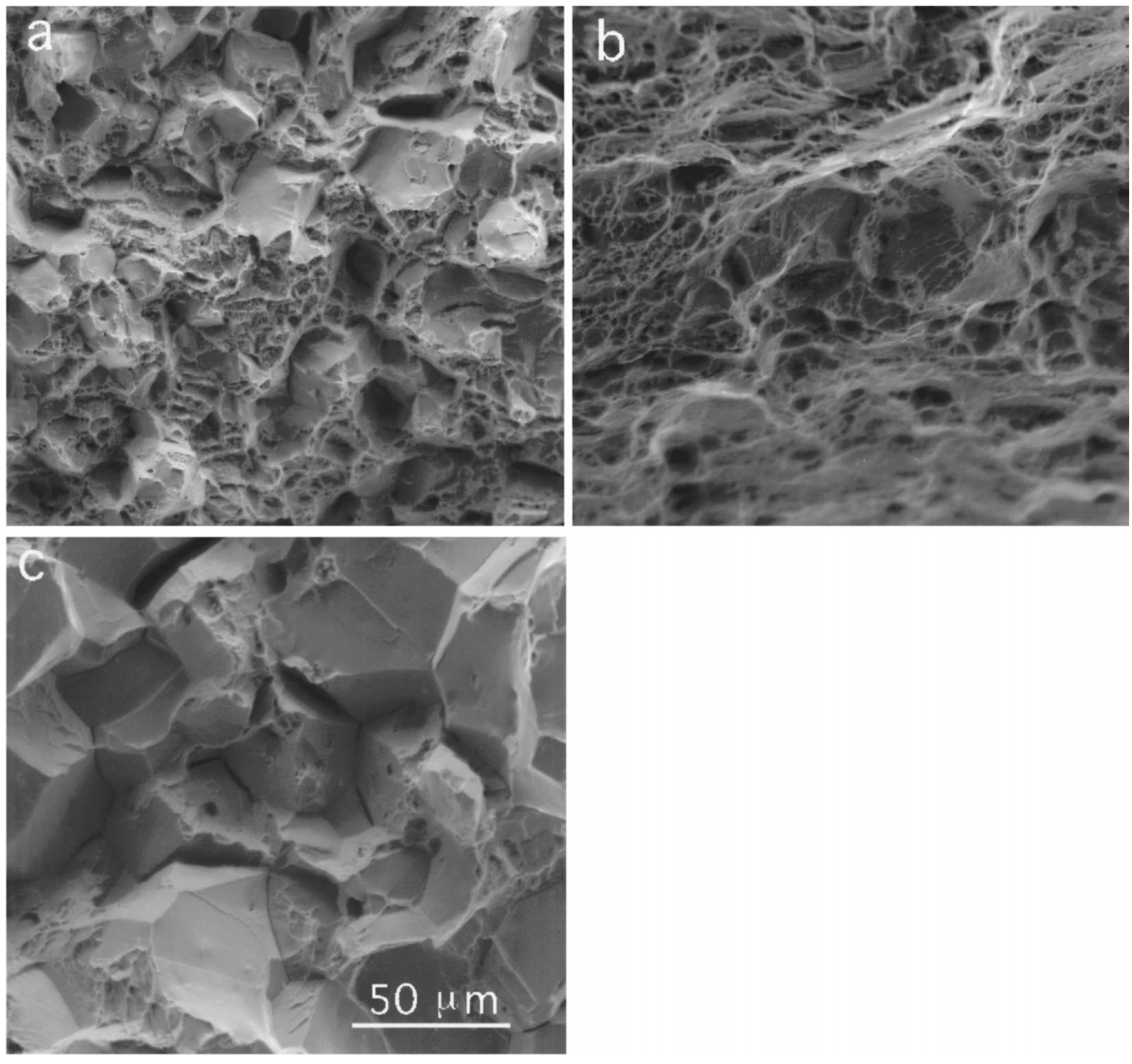

Figure 9 Variation with test temperature of fractographic patterns observed for the 2 at%Nb-added $Ni_3(Si,Ti)$ alloy. The tests were done at (a) room temperature, (b) 673 K and (c) 973 K.

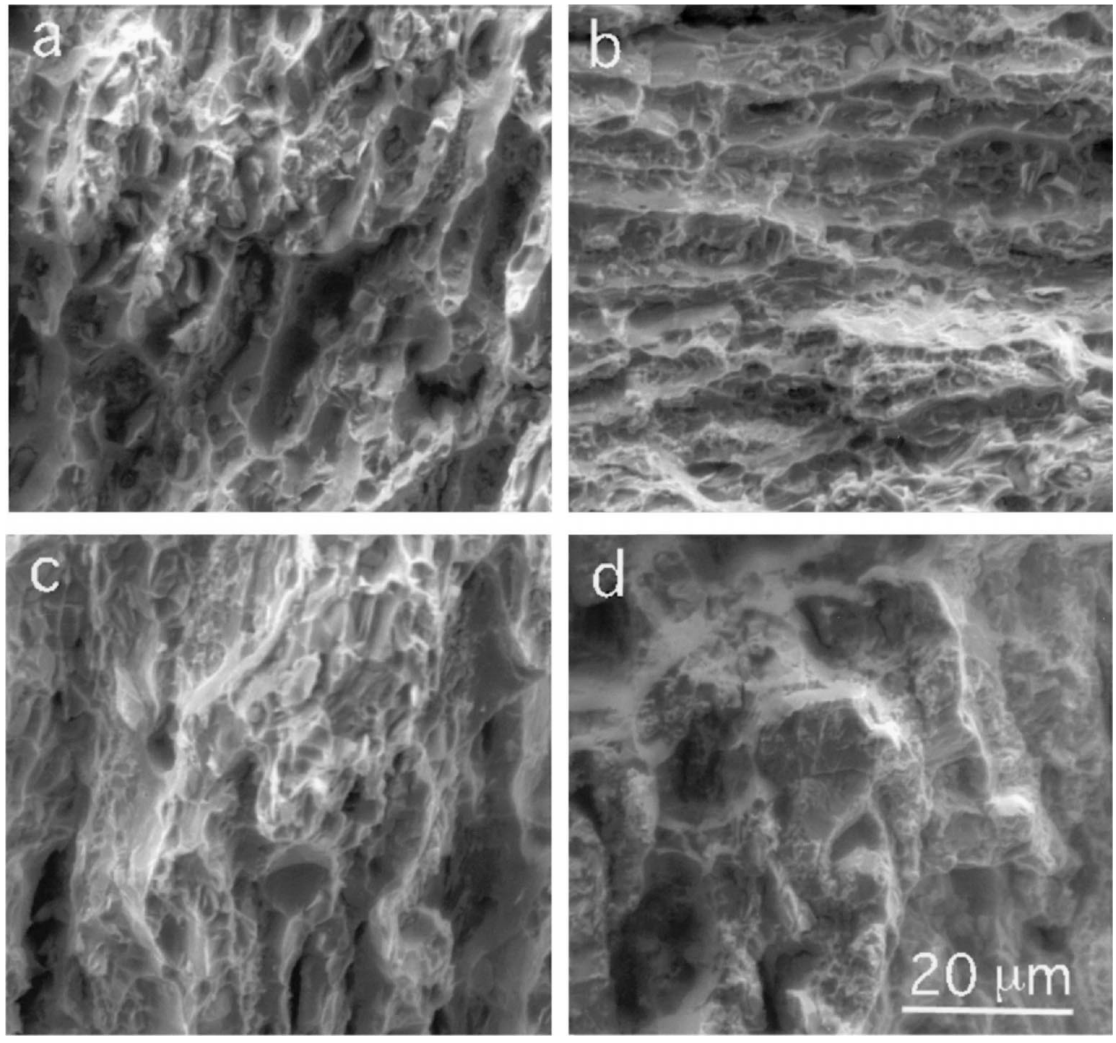

Figure 10 Variation with test temperature of fractographic patterns observed for the 4 at%Nb-added Ni_3(Si,Ti) alloy. The tests were done at (a) room temperature, (b) 673 K, (c) 873 K and (d) 1073 K.

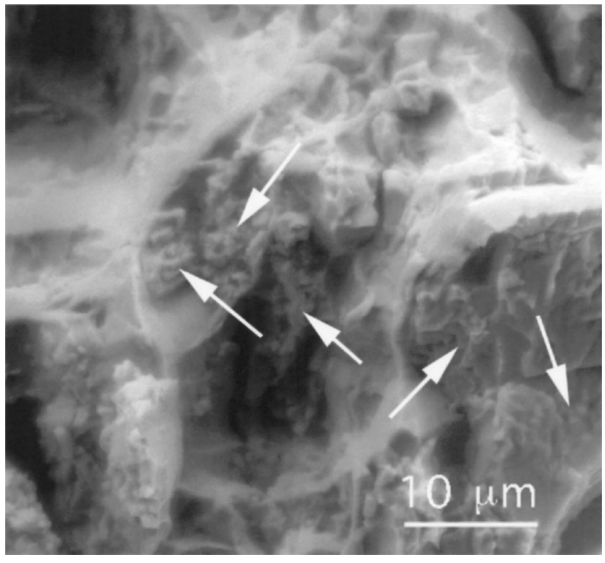

Figure 11 Fracture pattern taken at a high magnification for the 4 at%Nb-added Ni_3(Si,Ti) alloy tested at 1073 K. Dynamically recrystallized grains are denoted with 'arrow' marks.

4. Discussion

4.1. Phase relation and microstructure

The solubility limit of Nb element (∼2.7 at%) in the $L1_2$ Ni_3(Si,Ti) phase at 1273 K was determined to be smaller than that of Ti element (∼11 at%) [1]. However, this value is larger than those of most transition metals (e.g. V, Cr, Mn, Fe, Zr and Hf) [9]. To rationalize the solubility limits of quaternary elements X in $L1_2$ Ni_3A(A = Al,Si,Ga,Ge), Ochiai *et al*. [10] found a successful correlation between two parameters, i.e., the difference in the heats of compound formation between Ni_3A and Ni_3X, and the changing rate of lattice parameter on alloying of Ni_3A. To apply this to the present result, two hypotheses are required. The first hypothesis is that the quaternary element Nb should substitute for the A atom sites (i.e. the (Si,Ti) sites in this case). The second hypothesis is that the quaternary element Nb should furthermore be assumed not to interact with Ti. Experimental and theoretical observation has reported that Nb substitutes for the Si sites in the Ni_3Si alloy with a low solubility [9, 10]. Therefore, the two hypotheses can be satisfied for the Nb addition to the Ni_3(Si,Ti) alloy.

Fig. 12 represents a plot of the difference in the heats of compound formation between Ni_3Si and Ni_3X vs the atomic size difference between Si and quaternary element X. In this analysis, the changing rates of lattice parameter on alloying of Ni_3Si were replaced by the atomic size differences between Si and quaternary element X because no data are available for the changing

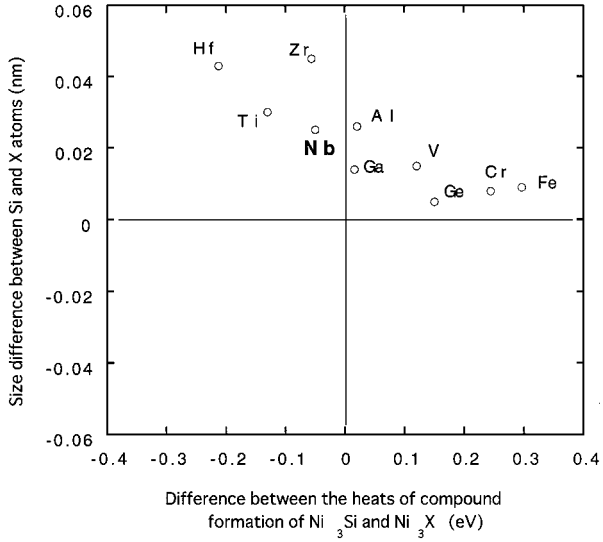

Figure 12 Atomic size misfit parameter between Si and quaternary element X in Ni_3Si *vs* the difference in the heats of compound between Ni_3Si and Ni_3X.

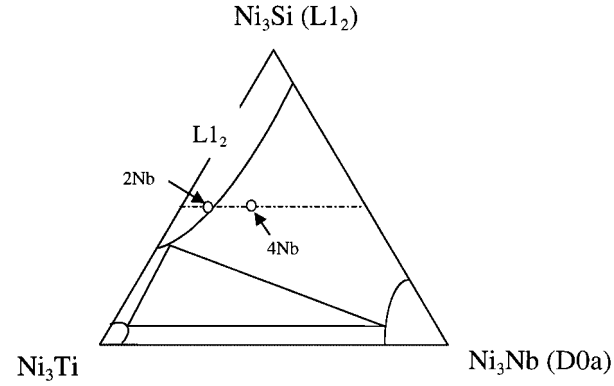

Figure 13 A proposed isothermal phase relation at 1273 K in the quaternary Ni-Si-Ti-Nb alloy system. Note that the phase relation is drawn in a pseudo-ternary alloy system, i.e. Ni_3Si-Ni_3Ti-Ni_3Nb. The data for three edge lines, i.e. Ni-Si-Ti, Ni-Si-Nb and Ni-Ti-Nb ternary alloy systems were obtained from the literatures [1, 10, 13], [10, 14] and [15], respectively.

rates of lattice parameter on alloying of Ni_3Si. Also, the heats of compound formation of Ni_3Si and Ni_3X were estimated using Miedema's formula [11]. Here, it is implicitly supposed that the maximum solubility is expected for the quaternary element X for which data points lie near the origin. Actually, the data points for Al, Ga and Ge that form continuous $L1_2$ solid solutions [10] fall near the origin. The data point for Nb is closer to the origin than the data points for Zr and Hf that showed small solid solubility in the $Ni_3(Si,Ti)$ [9, 12], and lie near the data points for Ti that showed large solid solubility in the $Ni_3(Si,Ti)$ [1]. Therefore, it is qualitatively concluded that the relatively large solubility limit of the Nb element in the $Ni_3(Si,Ti)$ alloy is attributed to (1) the relatively small difference in the heats of compound formation between Ni_3Si and Ni_3Nb and (2) the relatively small atomic size difference between Si and Nb elements.

Based on the metallograhic observation and the SEM-WDS analysis, a phase relation in the Ni-Si-Ti-Nb alloy system at 1273 K is qualitatively drawn in the form of a pseudoternary Ni_3Si-Ni_3Ti-Ni_3Nb phase diagram (Fig. 13). Here, currently available data for three edge lines, i.e. Ni-Si-Ti [1, 10, 13], Ni-Si-Nb [10, 14] and Ni-Ti-Nb [15] alloy systems are insufficient to complete this phase diagram. When Ni to X (= Si,Ti and Nb) ratio is thus kept identical (i.e. 3 : 1), three intermetallic compounds, Ni_3Si, Ni_3Ti and Ni_3Nb are formed, and consequently a single phase region, a two-phase region and a three-phase region are drawn depending on the prepared alloy compositions. Ternary intermetallic compounds may be formed. Actually, the Y-phase (defined as $Ni_{12}Si_4TiNb_2$ that is not able to plot on this pseudo-ternary Ni_3Si-Ni_3Ti-Ni_3Nb phase diagram) was observed in this study. More studies are necessary to completely construct the Ni-Si-Ti-Nb isothermal phase diagram.

The Ni_3Nb-based second-phase dispersion showed relatively large rounded shape with incoherent interface with the $L1_2$ $Ni_3(Si,Ti)$ matrix. Although the detailed phase diagram and the associated solidification process are not clear, the Ni_3Nb-based second-phase is assumed to be formed during solidification, i.e. from liquid. Therefore, it appears that the Ni_3Nb-based second-phase did not show any habit plane and coherent interface with the $L1_2$ $Ni_3(Si,Ti)$ matrix. Contrary to this result, finely distributed Ni_3Nb-based second phase dispersions was recently obtained by solid-state precipitation [16].

4.2. Mechanical behavior

The positive temperature dependence of the yield stress more or less decreased for the two Nb-added $Ni_3(Si,Ti)$ alloys, regardless of presence of the second-phase dispersions. It was shown that Ti in the $L1_2$ Ni_3Si matrix enhances a micro-cross slip of dislocation [17] resulting in the strength anomaly [2, 3, 4]. Replacement of Ti by Nb, both of which are dissolved in the Ni_3Si matrix as solute, may decelerate the micro-cross slip and instead enhances an athermal strength (i.e. solid solution hardening). The latter strength term does not contribute to the strength anomaly. Also, a part of this result may be attributed to the presence of the Ni_3Nb-based second-phase (dispersion).

As expected, the 4 at%Nb-added $Ni_3(Si,Ti)$ alloy was effectively strengthened by the Nb-containing second-phase dispersions at low temperatures. However, their morphology and size appear to be not always favorable for enhancing the flow stress. More attempts are needed to improve further the flow strength at low temperatures. As mentioned already, it was observed that the Nb-containing second-phase can be precipitated from the super-saturated $L1_2$ $Ni_3(Si,Ti)$ matrix, and thereby finely distributed Nb-containing second-phase dispersions were obtained [16]. Consequently, it is expected that more improved mechanical properties would be obtained for the Nb-added $Ni_3(Si,Ti)$ alloy with duplex microstructure consisting of $L1_2$ phase and finely precipitated Nb-containing second-phase dispersions.

The Nb-containing second-phases (dispersions) were shown to reduce the ductility (or UTS) at low temperatures. It is likely that the second-phase dispersions act as a stress enhancer, initiating premature

fracture by facilitating transgranular cracking. Therefore, finely distributed second-phase dispersions with coherency with the $Ni_3(Si,Ti)$ matrix may again be required to improve low temperature ductility as well as low temperature UTS.

At high temperatures, the Nb-containing second-phase dispersions were shown to improve the tensile elongation as well as UTS. In this temperature regime, the ductility is assumed to be influenced by competition between the two processes of grain boundary cavitation (or separation) and grain boundary migration [8]. The latter process is associated with dynamic recrystallization [8]. Here, it appears that the second-phase particles play an important role in the high temperature fracture process. As observed by SEM fractography (Fig. 11) and metallographic observation, dynamically recrystallized small grains were observed for the 4 at%Nb-added $Ni_3(Si,Ti)$ alloy deformed at high temperature. It is suggested that the second-phase dispersions provided easier nucleation sites to new grains and facilitated the growth of the new grains during high temperature deformation. New grains are considered to reduce the stress concentration at or near grain boundaries (or second-phase dispersions) and so enhance the ductility. In fact, the unalloyed $Ni_3(Si,Ti)$ did not show any propensity for dynamic recrystallization, and consequently did not display high elongation (and UTS) values at high temperature [4]. Again, it is expected that the size, morphology and coherency of the second-phase dispersion with the matrix would be important factors in affecting the dynamic recrystallization process and the resultant high temperature ductility.

Thus, the yield stress as well as UTS of the 4Nb-added $Ni_3(Si,Ti)$ alloy were significantly enhanced over a wide range of temperature, and in addition the tensile elongation of this alloy showed consistently high values without showing a ductility minimum at an intermediate temperature. Also, a recent study by the present author indicated that the Nb-added $Ni_3(Si,Ti)$ alloy with the Nb-containing second-phase dispersions was not susceptible to environmental embrittlement at all [9, 18], from which most unalloyed $Ni_3(Si,Ti)$ has so far been suffering [2, 4]. It has been reported that the Nb-containing second-phase dispersions are effective in preventing harmful hydrogen pick up from moisture in air [9, 18].

5. Conclusions

The alloying behavior, the microstructure and the high-temperature tensile properties of the Nb-added $Ni_3(Si,Ti)$ alloys were investigated by optical microscopy, scanning electron microscopy plus a wavelength dispersive spectroscopy, transmission electron microscopy and tensile testing. The following results were obtained.

1. The solubility limit of the Nb element in the $L1_2$ $Ni_3(Si,Ti)$ phase at 1273 K was approximately 2.7 at%, and thermodynamically discussed.

2. Two types of the second-phases (dispersions) were observed beyond the solubility limit. One was identified as the DO_a-type Ni_3Nb intermetallic compound, and contained lattice defect structures with incoherency with the $L1_2$ $Ni_3(Si,Ti)$ matrix. The other was defined as the $Ni_{12}Si_4TiNb_2$.

3. The Nb-containing second-phase dispersions in the $L1_2$ $Ni_3(Si,Ti)$ phase matrix resulted in strengthening over a wide range of temperature, and also an improvement of the high-temperature tensile elongation.

References

1. T. TAKASUGI, D. SHINDO, O. IZUMI and M. HIRABAYASHI, *Acta Metall. Mater*. **38** (1990) 739.
2. T. TAKASUGI, M. NAGASHIMA and O. IZUMI, *ibid*. **38** (1990) 747.
3. T. TAKASUGI, S. WATANABE, O. IZUMI and N. K. FAT-HALLA, *ibid*. **37** (1989) 3425.
4. M. YOSHIDA and T. TAKASUGI, *Phil. Mag*. **65** (1992) 41.
5. T. TAKASUGI, O. IZUMI and M. YOSHIDA, *J. Mater. Sci*. **26** (1991) 1173.
6. T. TAKASUGI, H. SUENAGA and O. IZUMI, *ibid*. **26** (1991) 1179.
7. T. TAKASUGI and M. YOSHIDA, *ibid*. **26** (1991) 3032.
8. *Idem*., *ibid*. **26** (1991) 3517.
9. T. TAKASUGI and S. HANADA, in "High-Temperature Ordered Intermetallic Alloys VIII," edited by E. P. George, M. J. Mills and M. Yamaguchi (MRS, 1999) p. 399. MRS Proc. Publ. Vol. 552.
10. S. OCHIAI, Y. OYA and T. SUZUKI, *Acta Metall*. **32** (1984) 289.
11. A. R. MIEDEMA, *J. Less-Common Metals* **46** (1976) 67.
12. T. TAKASUGI, *Materials Science and Technology* **16** (2000) 73.
13. P. VILLARS, A. PRINCE and OKAMOTO, "Handbook of Ternary Alloy Phase Diagrams" (ASM International, 1995) p. 13034.
14. *Idem*., *ibid*. p. 12799.
15. *Idem*., *ibid*. p. 12805.
16. T. TAKASUGI, unpublished work.
17. D. P. POPE and S. S. EZZ, *Int. Metals Rev*. **29** (1984) 136.
18. T. TAKASUGI and S. HANADA, *Intermetallics* **8** (2000) 47.

Received 16 September 1999
and accepted 28 February 2000